Geosci. Model Dev. Discuss., https://doi.org/10.5194/gmd-2018-287
Manuscript under review for journal Geosci. Model Dev.
Discussion started: 3 December 2018

Geoscientific Model Development Discussions

Vertically nested LES for high-resolution simulation of the surface layer in PALM (version 5.0)

Sadiq Huq[1], Frederik De Roo[1], Siegfried Raasch[3], and Matthias Mauder[1,2]

[1]Institute of Meteorology and Climate Research, Atmospheric Environmental Research (IMK-IFU), Karlsruhe Institute of Technology (KIT), Kreuzeckbahnstrasse 19, 82467 Garmisch-Partenkirchen, Germany
[2]Institute of Geography and Geoecology (IfGG), Karlsruhe Institute of Technology, Kaiserstrasse 12, 76131 Karlsruhe, Germany
[3]Institute of Meteorology and Climatology, Leibniz Universität Hannover, Hannover, Germany

Correspondence to: matthias.mauder@kit.edu

Abstract. Large-eddy simulation (LES) has become a well-established tool in the atmospheric boundary-layer research community to study turbulence. It allows three-dimensional realizations of the turbulent fields, which large-scale models and most experimental studies cannot yield. To resolve the largest eddies in the mixed layer, a moderate grid resolution in the range of 10 to 100 m is often sufficient, and these simulations can be run on a computing cluster with few hundred processors, or even on a workstation for simple configurations. The desired resolution is usually limited by the computational resources. However, to compare with tower measurements of turbulence and exchange fluxes in the surface layer a much higher resolution is required. In spite of the growth in computational power, a high-resolution simulation LES of the surface layer is often not feasible: to fully resolve the energy containing eddies near the surface a grid spacing of O(1 m) is required. One way to tackle this problem is to employ a vertical grid nesting technique, where the surface is simulated at the necessary fine grid resolution, and it is coupled with a standard, coarse, LES that resolves the turbulence in the whole boundary-layer. We modified the LES model PALM (Parallelized Large-eddy simulation Model) and implemented a two-way nesting technique, with coupling in both directions between the coarse and the fine grid. The coupling algorithm has to ensure correct boundary conditions for the fine grid. Our nesting algorithm is realized by modifying the standard third order Runge-Kutta time stepping to allow communication of data between the two grids. The two grids are concurrently advanced in time while ensuring that the sum of resolved and subgrid-scale kinetic energy is conserved. We design a validation test and show that the temporal averaged profiles from the fine grid agree well compared to the reference simulation with high-resolution in the entire domain. The overall performance and scalability of the nesting algorithm is found to be satisfactory. Our nesting results in more than 80 percent savings in computational power for 5 times higher resolution in each direction in the surface layer.

Geosci. Model Dev. Discuss., https://doi.org/10.5194/gmd-2018-287
Manuscript under review for journal Geosci. Model Dev.
Discussion started: 3 December 2018

Geoscientific Model Development Discussions

1 Introduction

Turbulence in the Atmospheric Boundary Layer (ABL) encompasses a wide range of scales from the boundary-layer scale down to the viscous dissipation scale. In ABL flows, Reynolds numbers (Re) of 10^8 are commonly encountered. Explicit simulation of the Navier-Stokes equations down to the dissipative scales (DNS: direct numerical simulation) for atmospheric processes is prohibitively expensive, as the required number of grid points in one direction scales with $Re^{3/4}$ (Reynolds, 1990). This corresponds to a three-dimensional ABL simulation domain with total number of grid points of order 10^{17}. The supercomputers of today cannot fit more than 10^{12} grid points in the memory. To be able to compute turbulence processes in the atmosphere nevertheless, the concept of large-eddy simulation (LES) has been introduced already a few decades ago, e.g. Deardorff (1974); Moeng and Wyngaard (1988); Schmidt and Schumann (1989), where the presence of a subgrid-scheme allows that only the most energetic eddies are resolved.

One of the first large-eddy simulations (LES) by Deardorff (1974) used 64000 grid points to simulate a domain of $5\ \mathrm{km} \times 5\ \mathrm{km} \times 2\ \mathrm{km}$ with a grid resolution of $(125, 125, 50)\ \mathrm{m}$. The size of one such grid cell is just sufficient to resolve the dominant large-eddies and there are just enough grid points to represent the ABL. As computing power progressed, higher resolution and larger domains became possible, by the time of Schmidt and Schumann (1989) the number of grid cells had raised to $160 \times 160 \times 48$ simulating an ABL of $8\ \mathrm{km} \times 8\ \mathrm{km} \times 2.4\ \mathrm{km}$ with a resolution of $(50, 50, 50)\ \mathrm{m}$. Khanna and Brasseur (1998) used 128^3 grid points to simulate a domain of $3\ \mathrm{km} \times 3\ \mathrm{km} \times 1\ \mathrm{km}$ to study buoyancy and shear induced local structures of the ABL. Patton et al. (2016) used $(2048, 2048, 1024)$ grid points with a grid resolution of $(2.5, 2.5, 2)\ \mathrm{m}$ to study the influence of atmospheric stability on canopy turbulence. More recently, with the help of supercomputers, Kröniger et al. (2018) used $13 \cdot 10^9$ grid points to simulate a domain of $30.72\ \mathrm{km} \times 15.36\ \mathrm{km} \times 2.56\ \mathrm{km}$ to study the influence of wind speeds on the surface–atmosphere exchange and the role of secondary circulations in the energy exchange. The atmospheric boundary-layer community has greatly benefited from the higher detail available in these LES to study turbulent processes that cannot be measured in the field in three-dimensional detail.

Still, especially in heterogeneous terrain, near topographic elements, buildings or close to the surface the required higher resolution is not always attainable. Considering the size of the domain required to reproduce boundary-layer scale structures, it is challenging to generate a single fixed grid that could resolve all the relevant scales satisfactorily. In spite of the radical increase in the available computing power, Large-Eddy Simulation of atmospheric flows with very high-resolution in the surface-layer continue to be computationally expensive. However, grid nesting technique can be employed to reduce the number of grid points required. To resolve the surface-layer a vertical nesting technique is needed. Nesting has been applied to several mesoscale models (Skamarock et al., 2008; Debreu et al., 2012) , but, in contrast to horizontal nesting, vertical nesting is less common. In the nested grid approach, a parent domain with a coarser resolution simulates the entire domain while a nested grid with a higher resolution extends only up to the region of interest. Horizontally nested LES-within-LES or LES embedded within a mesoscale simulation is available in the Weather Research and Forecast model (Moeng et al., 2007). However, we would like to point out that the vertical nesting in WRF (Daniels et al., 2016) is not a conventional vertical nesting because the parent and the child grid still have the same vertical extent, the child grid is only more refined in the vertical. A non-parallelized

Geosci. Model Dev. Discuss., https://doi.org/10.5194/gmd-2018-287
Manuscript under review for journal Geosci. Model Dev.
Discussion started: 3 December 2018

vertical nesting was explored by (Sullivan et al., 1996) but the code is not in public domain and we could not find any record of further development or application of this code in publications. An LES-within-LES vertical nesting is implemented by Zhou et al. (2018) in the Advanced Regional Prediction System (ARPS) model. Comparable grid nesting techniques are also widely employed by the engineering turbulence research community but often uses different terminology. Nesting in codes with cartesian grids are referred as local or zonal grid (Kravchenko et al., 1996; Boersma et al., 1997; Manhart, 2004) and as overset mesh (Nakahashi et al., 2000; Kato et al., 2003; Wang et al., 2014) in unstructured or moving grid codes.

For our purposes, we will focus on vertical nesting, i.e. we consider a finer grid near the lower boundary of the domain, and a coarser grid in the remainder of the boundary layer. While the latter's resolution ($< 50\,\mathrm{m}$) is sufficient to study processes in the outer region where the dominant eddies are large and inertial effects dominate, such coarse resolution is not sufficient when fine-scale turbulence in the surface layer region is concerned. The higher resolution achieved by the vertical nesting there will then allow a more accurate representation of the turbulence in the surface layer region by resolving its dominant eddies. For studies that require very high resolution near the surface (e.g. tower measurements, wakes behind obstacles, dispersion within street canyons for large cities) a nesting approach is an attractive solution due to the reduced memory requirement. An increased resolution only in the surface-layer can be achieved by a LES-within-LES set-up by maintaining the same horizontal extent for the Fine Grid nested domain (FG) and the Coarse Grid parent domain (CG). The challenge of a vertically nested grid is that the FG upper boundary conditions need to be correctly prescribed by the CG.

An analysis of different nesting procedures for mesoscale simulation was performed by Clark and Hall (1991), they coined the terms one-way and two-way interactions. In one-way interaction, only the FG receives information from the CG, there is no feedback to the CG. In two-way interaction, the FG top boundary conditions are interpolated from the CG and the CG values in the overlapping region are updated with the FG resolved fields. The 'update' process, referred to as 'anterpolation' by Sullivan et al. (1996) is similar to the restriction operation in Multi-Grid methods. Harris and Durran (2010) used a linear 1D shallow-water equation to study the influence of the nesting method on the solution and found the two-way interaction to be superior when the waves are well resolved. We will make use of the interpolation and anterpolation formulas of Clark and Farley (1984). Clark and Hall (1991) studied two different approaches for updating the CG values namely, "Post-insertion" and "Pressure Deficit Correction". In the post-insertion technique, once the Poisson equation for pressure is solved in the FG, the resolved fields are then anterpolated to the CG. Though, they note the latter approach to be more elegant, no significant difference in the results was reported. Moreover, only the post-insertion technique permits different temporal resolution in the FG and CG. Sullivan et al. (1996) report that in the case of their Pseudo-Spectral LES, both the resolved and SGS fluxes need to be anterpolated to the CG and such a procedure increases coding complexity.

In the following sections we describe the technical realization and numerical aspects of the two-way nesting algorithm. In the LES model PALM, a validation simulation is set-up and the results of the nested and standalone simulations are compared. A second simulation is set-up to evaluate the computational performance of the algorithm. The practical considerations and the limitations of the two-way nesting are then discussed.

Geosci. Model Dev. Discuss., https://doi.org/10.5194/gmd-2018-287
Manuscript under review for journal Geosci. Model Dev.
Discussion started: 3 December 2018

Geoscientific Model Development Discussions
Open Access
EGU

2 Methods

2.1 Description of the standard PALM Model

The Parallelized Large-eddy simulation Model (PALM) is developed and maintained at the Leibniz University of Hannover (Raasch and Schröter, 2001; Maronga et al., 2015). We give a quick summary of the model here and highlight the aspects which will reappear when discussing our nesting modifications. For a thorough description of the model, see Maronga et al. (2015). PALM is a Finite Difference solver for the non-hydrostatic incompressible Navier-Stokes equations in the Boussinesq approximation (Eqs. 1, 2, and 3). PALM solves for six prognostic equations: the three components of the velocity field (u, v, w), potential temperature (θ), humidity (q) and the sub-grid scale kinetic energy (e). The sub-grid scale (SGS) turbulence is based on the method proposed by Deardorff (1980) with an additional equation for the turbulent kinetic energy. The 1.5 order closure parameterization modified by Moeng and Wyngaard (1988) and Saiki et al. (2000), assumes a gradient diffusion parameterization (Eq. 4). The prognostic equations are discretized on a staggered Arakawa C-grid, where the scalars are evaluated in the center of the grid volume and velocities are evaluated at the center of the faces of the grid volume in their respective direction.

$$\frac{\partial \overline{u}_i}{\partial t} = -\frac{\partial \overline{u}_k \overline{u}_i}{\partial x_k} - \frac{1}{\rho_0}\frac{\partial \overline{\pi}^*}{\partial x_i} - \varepsilon_{ijk} f_j \overline{u}_k + \varepsilon_{i3k} f_3 \overline{u}_{k_g} + g\frac{\overline{\theta} - \theta_0}{\theta_0}\delta_{i3} + \nu\frac{\partial^2 \overline{u}_i}{\partial x_k^2} - \frac{\partial \tau^r_{ki}}{\partial x_k}. \tag{1}$$

$$\frac{\partial \overline{u}_k}{\partial x_k} = 0. \tag{2}$$

$$\frac{\partial \overline{\theta}}{\partial t} = -\frac{\partial \overline{u}_k \overline{\theta}}{\partial x_k} - \frac{\partial H_k}{\partial x_k} + Q_\theta. \tag{3}$$

$$\frac{\partial \overline{e}}{\partial t} = -\overline{u}_k \frac{\partial \overline{e}}{\partial x_k} - \tau_{ki}\frac{\partial \overline{u}_i}{\partial x_k} + \frac{g}{\theta_0}\overline{u_3'\theta'} - \frac{\partial}{\partial x_k}\left\{\overline{u_k'\left(e' + \frac{\pi'}{\rho_0}\right)}\right\} - \epsilon. \tag{4}$$

The advection terms are evaluated either with fifth-order upwind discretization according to Wicker and Skamarock (2002) or with a 2nd order scheme according to Piacsek and Williams (1970). The prognostic equations are integrated in time using a third-order Runge-Kutta (RK3) scheme. The low storage RK3 scheme with three sub-steps proposed by Williamson (1980) guarantees a stable numerical solution. The Poison Equation for pressure is solved with Fast-Fourier Transform (FFT) when periodic boundary conditions are applied in the lateral boundaries. There are three FFT algorithms available in PALM with FFTW being the optimal method for large scale simulations. Monin-Obukhov Similarity Theory (MOST) is assumed between the surface and the first grid point. A zero pressure gradient at the surface guarantees vertical velocity to be zero. Simulations can be driven by either prescribing the surface temperature or the surface heat flux, similarly for the humidity. At the top of the simulation domain the horizontal velocities equal geostrophic wind and the vertical velocity is set to zero. The pressure can

Geosci. Model Dev. Discuss., https://doi.org/10.5194/gmd-2018-287
Manuscript under review for journal Geosci. Model Dev.
Discussion started: 3 December 2018

assume either a Dirichlet condition of zero value or a Neumann condition of zero vertical gradient. The scalar values have a fixed gradient. The vertical gradient of SGS Turbulent Kinetic Energy (TKE) is set to zero at both top and bottom boundaries.

PALM is a parallelized model and the standard way of parallelization is by dividing the three-dimensional domain into vertical columns, each of which is assigned to one processing element (PE). Each vertical column possesses a number of ghost points needed for computation of derivatives at the boundary of the sub-domains. Each PE can only access data for a single sub-domain. All PEs execute the same program on a different set of data. For optimum load balancing between the PE the decomposed sub-domains should have the same size. In PALM, this condition is always satisfied as only sub-domains of the same size are allowed. After every time-integration step, the data exchange between PEs, needed to update the ghost points, is performed via the Message Passing Interface (MPI) communication routines.

2.2 Fine grid and coarse grid configuration

We are interested in achieving an increased resolution only in the surface-layer, the lowest 10% of the boundary layer, where surface exchange processes occur and where eddies generated by surface heterogeneity and friction are smaller than the dominant eddies in the mixed layer. We setup the LES-within-LES case by maintaining the same horizontal extent for the FG and the CG to have the whole surface better resolved. We allow the vertical extent of the FG to be varied as needed, typically up to the SL depth. This implementation of vertical grid nesting has two main challenges. The first challenge, that is purely technical in nature, is to implement routines that handle the communication of data between the CG and the FG. The second and the most important challenge is to ensure that the nesting algorithm yields an accurate solution in both the grids.

The nesting ratio is defined as the ratio of the CG spacing to the FG spacing, $n_x = \Delta X/\Delta x$, corresponding symbols apply for y and z directions. The nesting ratios n_x, n_y and n_z have to be integer. It is possible to have either odd or even nesting ratio and it can be different in each direction. As the domain that is simulated in the FG is completely inside of the CG domain, each FG cell belongs to a CG cell. The two grids are positioned in such a way that a FG cell belongs to only one CG cell and one CG cell is made up by a number of FG cells given by the product of the nesting ratios $n_x \times n_y \times n_z$. This means that if the grid nesting ratio is odd, there will be one FG cell whose center is exactly at the same position as the center of the coarse cell. The collection of FG cells that correspond to one CG cell is denoted by $\mathcal{C}(I, J, K)$, the collection of FG faces that corresponds to e.g. an yz-face of the CG $\mathcal{C}_x(I_s, J, K)$, where it is understood that the I_s index is an index on the staggered grid in the x-direction to denote the position of the face, and similar for the other types of faces. Below we use upper case symbols for fields and variables in the CG, and lower case for the FG. E.g. E and e denote the subgrid-scale turbulent kinetic energy (a prognostic variable in our LES) of CG and FG respectively. We have used $f_x = 1/n_x$ to denote the inverse of the nesting ratio in the x dimension (corresponding symbols for y and z). A schematic diagram of the overlapping grids are shown in Fig. 1.

For the boundary conditions at the top of the FG, the fields from the CG are interpolated to the FG, according to Clark and Farley (1984). In Eq. 5, Φ and ϕ represent CG and FG quantities, respectively. For the scalar fields, the interpolation is quadratic in all three directions. For the velocity components, the interpolation is linear in the logical direction of that component, and

Geosci. Model Dev. Discuss., https://doi.org/10.5194/gmd-2018-287
Manuscript under review for journal Geosci. Model Dev.
Discussion started: 3 December 2018

Geoscientific Model Development Discussions
Open Access
EGU

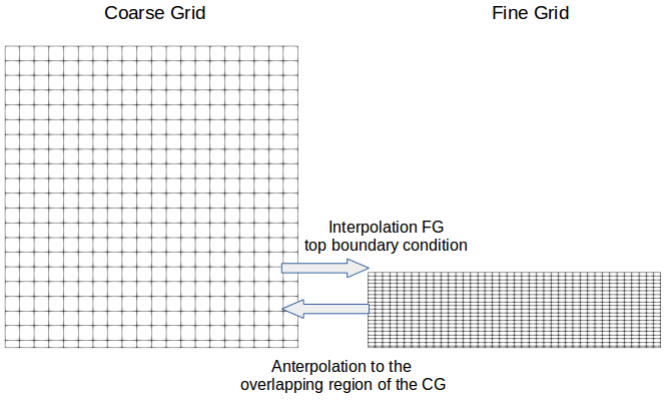

Figure 1. Schematic of the interpolation and anterpolation between the grids. The FG top boundary condition is interpolated from the CG. The CG prognostic quantities in the overlapping region are anterpolated from the FG.

quadratic in the other two directions. A similar interpolation is carried out for the initialization of the fine grid. The quadratic interpolation equation reads as

$$
\begin{aligned}
\phi_i &= \eta^i_- \Phi_{I-1} + \eta^i_0 \Phi_I + \eta^i_+ \Phi_{I+1}, \\
\eta^i_- &= \frac{1}{2} H_k (H_k - 1) + \alpha, \\
\eta^i_0 &= (1 - H_k^2) - 2\alpha, \\
\eta^i_+ &= \frac{1}{2} H_k (H_k + 1) + \alpha, \\
H_i &= \frac{1}{2}((2i-1) f_x - 1), \\
\alpha &= \frac{1}{24}\left(f_x^2 - 1\right).
\end{aligned}
\tag{5}
$$

The anterpolation of the prognostic quantities are performed by an averaging procedure according to Clark and Hall (1991). The scalars are defined as the spatial average over the whole grid cell, therefore it is required that the CG scalar is the average of the corresponding FG scalars (Eq. 6). However, the CG velocity components are the average of only the FG value at the corresponding faces (Eq. 7). The anterpolation equations read as

$$
\Phi_{I,J,K} = [\phi]_{i,j,k} = \sum_{i,j,k} \phi_{i,j,k} f_x f_y f_z. \tag{6}
$$

Geosci. Model Dev. Discuss., https://doi.org/10.5194/gmd-2018-287
Manuscript under review for journal Geosci. Model Dev.
Discussion started: 3 December 2018

Geoscientific Model Development Discussions

$$
\begin{aligned}
U_{I,J,K} &= < u >_{j,k} = \sum_{j,k} u_{i,j,k} f_y f_z, \\
V_{I,J,K} &= < v >_{i,k} = \sum_{i,k} v_{i,j,k} f_x f_z, \\
W_{I,J,K} &= < w >_{i,j} = \sum_{i,j} w_{i,j,k} f_x f_y.
\end{aligned}
\tag{7}
$$

However, the TKE in the CG differs from the FG value. Due to the different resolution of the grids, in the FG the SGS motions are weaker. Therefore, TKE is anterpolated such that the Germano identity is maintained (Germano et al., 1991):

$$
E = [e] + \frac{1}{2} \sum_{i,j \in \mathcal{C}} \left([u_i u_j] - [u_i][u_j] \right). \tag{8}
$$

2.3 Summary of the Nesting Algorithm

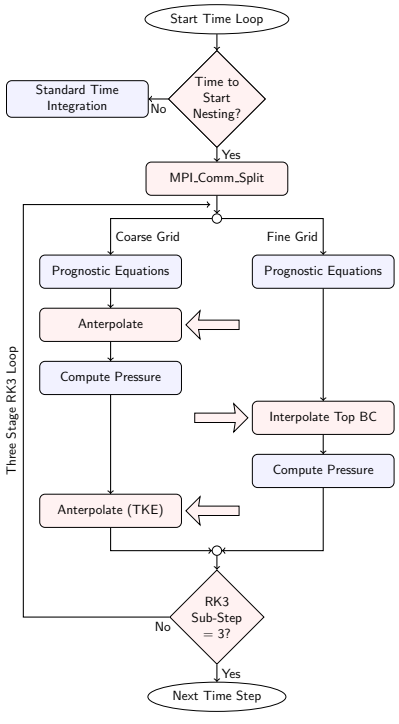

Figure 2. A flowchart of the two-way interaction algorithm. The new routines needed for the vertical nesting are highlighted in red and the standard routines are highlighted in blue. An arrow pointing to the left indicates transfer of data from FG to CG, and vice versa.

We implement a two-way interaction algorithm, shown in Fig. 2, because in our first trials we found that one-way nesting did not improve the FG representation satisfactorily and hence was not pursued further. The FG prognostic quantities are initialized

Geosci. Model Dev. Discuss., https://doi.org/10.5194/gmd-2018-287
Manuscript under review for journal Geosci. Model Dev.
Discussion started: 3 December 2018

by interpolating the CG values in the overlapping region. Optionally, the initialization of the FG can be delayed until the CG has reached a fully turbulent state. Both the grids are restricted to have identical time steps. PALM finds the largest time step for each grid such that the CFL condition is individually satisfied and the minimum of the two values is then chosen as the time integration step for both the grids. The right hand side of the prognostic equation except for the pressure is first computed concurrently in both the grids. The values of u, v, w, θ and q are then anterpolated to the CG in the overlapping region. The CG solves a Poisson equation for pressure. The new u, v, w, θ and q fields in the CG are interpolated to set the FG Dirichlet top boundary conditions. The Poisson equation is then solved for pressure in the FG and the vertical velocity is also updated by the pressure solver at this stage. The TKE is then anterpolated maintaining the Germano identity and it is followed by the computation of SGS eddy diffusivity for heat (k_h) and momentum (k_m) in the CG. This procedure is repeated at every sub-step of the Runge-Kutta 3 time integration and it ensures that the velocity field remains divergence free in both the grids. Since all the velocity components follow Dirichlet condition at FG top boundary only Neumann condition is suitable for Pressure (Manhart, 2004). PALM permits the use of Neumann condition for pressure at both top and bottom boundary. It is advisable to use Neumann boundary condition at top and bottom for the CG too.

2.4 Parallel Inter-Grid Communication

MPI is the most widely used large scale parallelization library. The atmosphere-ocean coupling in PALM has been implemented following MPI-1 standards (Esau, 2014; Maronga et al., 2015). We follow a similar approach for the MPI communications, and have adopted MPI-1 standards for our nesting implementation. Concurrent execution of the two grids is achieved with the MPI_COMM_SPLIT procedure. The total available processors are split into two groups, denoted by color 0 or 1 for CG and FG respectively, see Fig. 3. The data between the processors of the same group are exchanged via the local communicator created during the splitting process. Whereas, the data between the two groups are exchange via the global communicator MPI_COMM_WORLD.

Based on the nesting ratio and the processor topology of the FG and the CG group a mapping list is created and stored. Given the local PE's 2D processor co-ordinate – the list will identify the PEs in the remote group to/from which data needs to be sent/received; the actual communication then takes place via the global communicator.

There are three types of communication in the nesting scheme:

i. Initializing the FG (Send data from coarse grid to fine grid.) This is performed only once.

ii. Boundary condition for the FG top face (Send data from coarse grid to fine grid.).

iii. Anterpolation (Send data from fine grid to coarse grid.).

The exchange of arrays via MPI_SENDRECV routines is computationally expensive. Therefore, the size of the arrays communicated are minimized by performing the anterpolation operation in the FG PE's and storing the values in a temporary 3D array that is later sent via the global communicator to the appropriate CG PE. This approach also takes advantage of the higher number of PE available in the FG. Furthermore, the array data that need to be communicated during the anterpolation operation and for setting the FG boundary condition are not contiguous in memory. The communication performance is enhanced by creating an MPI derived data type that ensures that the data is sent contiguously. Within the RK3 sub-steps, when one grid

Geosci. Model Dev. Discuss., https://doi.org/10.5194/gmd-2018-287
Manuscript under review for journal Geosci. Model Dev.
Discussion started: 3 December 2018

Geoscientific Model Development Discussions

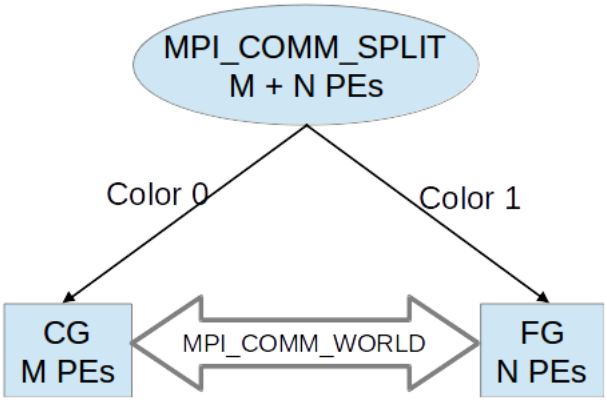

Figure 3. Schematic of the MPI processor grouping. The data exchange between the two groups are performed via the global communicator. M and N are the number of processors for CG and FG respectively.

executes the pressure solver the other grid has to wait leading to more computational time at every sub-step. However, the delay can be minimized by effective load balancing, i.e. the number of grid points per PE in the CG should be kept lower than in the FG. This reduction in workload per PE can be achieved with just a few additional cores.

3 Results and Discussion

3.1 Simulation set-up for the nesting validation test

To evaluate the accuracy of the two-way nesting algorithm we set-up a convective boundary layer simulation. Two overlapping grids with a nesting ratio of five in the lateral and vertical direction are employed. The simulation parameters are listed in Table 1. A standalone reference simulation with the same resolution as the coarse grid (SA-C) and another reference with the same resolution as the fine grid (SA-F) are performed for comparison. The grid configuration and the computational resources used are listed in Table 2. The simulations were performed in a local computing cluster, each compute node has 64 GB of main memory and a 2.8 GHz Ivy Bridge processor with 20 cores. The simulation domain is set to periodic boundary conditions in the lateral direction. At the top and bottom boundaries, the velocity components are set to Dirichlet condition, the pressure and humidity are set to Neumann condition. The potential temperature is set to Neumann condition at the bottom and the gradient of the initial profile is maintained at the top boundary. In PALM, u_g and v_g represents the u- and v-component of the geostrophic wind at the surface. The u and v profiles are constructed starting from a zero value at the surface and reaches the geostrophic wind value at the top. The vertical velocity is initialized to zero in the domain. The potential temperature is initialized to a constant value of 300 K up to 800 m and above 800 m a lapse rate of 1 K 100 m^{-1} is prescribed. The humidity

Geosci. Model Dev. Discuss., https://doi.org/10.5194/gmd-2018-287
Manuscript under review for journal Geosci. Model Dev.
Discussion started: 3 December 2018

Geoscientific Model Development Discussions

profile is initialized to a constant value of 0.005 $\mathrm{kg\ kg^{-1}}$. The simulation is driven by prescribing a surface heat flux of 0.1 $\mathrm{Kms^{-1}}$ and a surface humidity flux of 4 x 10^{-4} $\mathrm{kgkg^{-1}ms^{-1}}$.

Table 1. Simulation Parameters for the nesting validation test.

Domain Size:	4.0 x 4.0 x 1.65 $\mathrm{km^3}$
Fine grid vertical extent:	320 m
Kinematic surface heat flux:	$w'\theta'_0$ = 0.1 $\mathrm{Kms^{-1}}$
Kinematic surface humidity flux:	$w'q'_0$ = 4 x 10^{-4} $\mathrm{kgkg^{-1}ms^{-1}}$
Geostrophic wind:	u_g = 1 $\mathrm{ms^{-1}}$, v_g = 0 $\mathrm{ms^{-1}}$
Simulated time:	10800 s
Spin-up time:	9000 s
Averaging interval:	1800 s

Table 2. Grid configuration of the nested and standalone reference domains.

	No. of Grid Points	(dx,dy,dz) m	cpu cores	core-hours
Coarse Grid (CG)	200 x 200 x 80 = 3.2 x 10^6	20, 20, 20	20	290
Fine Grid (FG)	1000 x 1000 x 80 = 80 x 10^6	4, 4, 4	80	1160
Total				1450
Standalone Coarse (SA-C)	200 x 200 x 80 = 3.2 x 10^6	20, 20, 20	20	5
Standalone Fine (SA-F)	1000 x 1000 x 400 = 400 x 10^6	4, 4, 4	400	10345

3.2 Analysis of the simulations

In a two-way nesting it is important that the flow structures are propagated from the FG to CG and vice versa, without any distortion. In Fig. 4, the contours in the CG region overlapping the FG have similar structures as the FG. The higher resolution in the FG enables more detailed contours whereas the anterpolated CG contours are smoother. Furthermore, in the CG region beyond the overlapping region no distortion to the contours are observed indicating that the anterpolation does not introduce sharp gradients in the CG.

Geosci. Model Dev. Discuss., https://doi.org/10.5194/gmd-2018-287
Manuscript under review for journal Geosci. Model Dev.
Discussion started: 3 December 2018

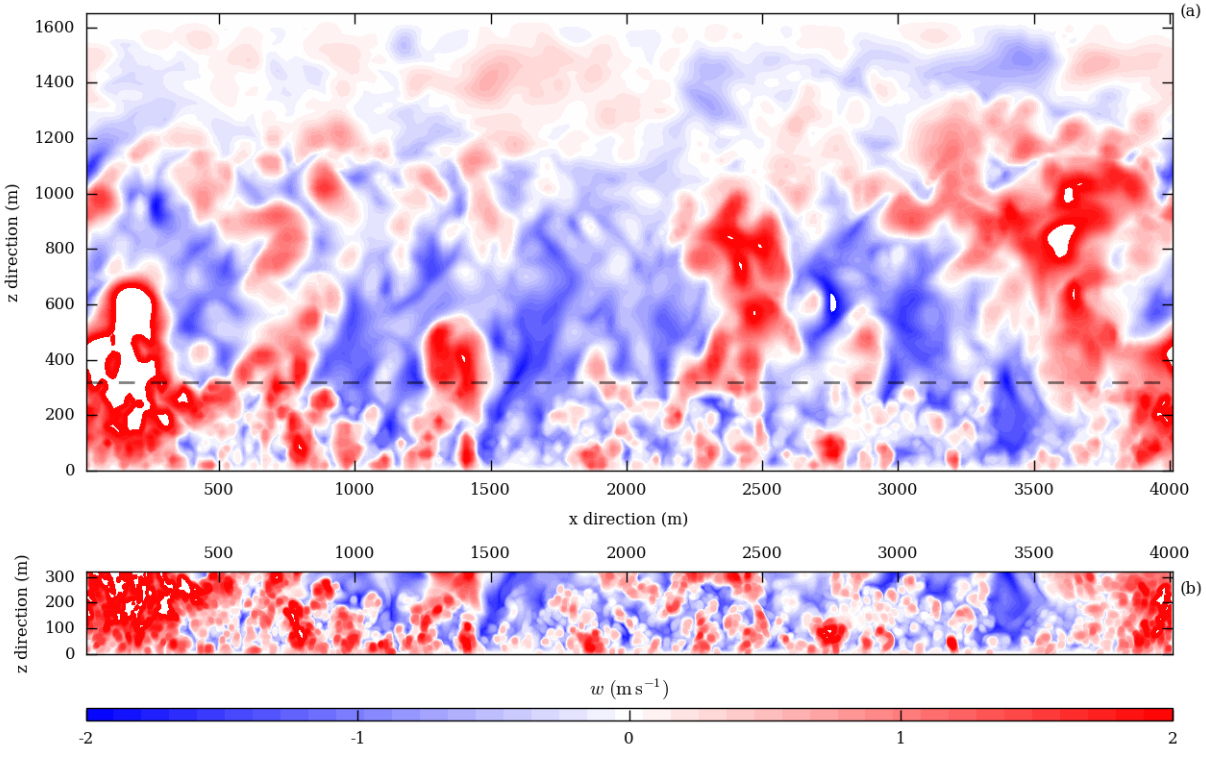

Figure 4. Instantaneous contours of vertical velocity, (a) CG and (b) FG, at the vertical x-z cross-section at the center of the domain after 9000 s of the simulation. The dashed line in (a) marks the top of the overlapping region. Flow structures in the FG, are similar but more detailed than the CG, qualitatively indicate the improvement to the surface-layer resolution with the two-way nesting.

The vertical profiles are used for quantitative comparison of the nested and the reference simulations. The turbulent fluctuations (e.g. θ'',w'') are defined as the spatial deviations from the instantaneous horizontal average. The turbulent flux profiles (e.g. $w''\theta''$, $u''u''$) are obtained using the spatial covariance and are then horizontally averaged. All the horizontally averaged profiles (e.g. $<\theta>$, $<w''\theta''>$) are also averaged over time but we omit the conventional overline notation for simplicity. The friction velocity (u_*), convective velocity scale (w_*) and temperature scale (θ_*) obtained from SA-F are used to normalize the profiles. The convective velocity is calculated as $w_* = (g\ \theta_0^{-1}\ w'\theta'_0\ z_i)^{1/3}$, where g is the gravitational acceleration, θ_0 is the surface temperature and z_i is the boundary layer height in the simulation. The convective temperature scale is calculated as $\theta_* = w'\theta'_0\ w_*^{-1}$. The vertical profiles of potential temperature ($<\theta>$) normalized by the surface value are shown in Fig. 5 (a and c). Since the FG profiles are superior to the CG in the over-lapping region, the anterpolated CG values are not plotted. In Fig. 5 (a), there is no visible difference between the standalone and the nested simulations. However, in the region closer to the surface, plotted in Fig. 5 (c), a better agreement between the SA-F and FG is observed. The potential temperature variance ($<\theta''\theta''>$) normalized by the square of the temperature scale (θ_*^2) are shown in Fig. 5 (b and d). Here too FG provides better accuracy close to the surface. It is important to note in Fig. 5 (b), at the boundary layer height well above the overlapping

Geosci. Model Dev. Discuss., https://doi.org/10.5194/gmd-2018-287
Manuscript under review for journal Geosci. Model Dev.
Discussion started: 3 December 2018

Geoscientific Model Development Discussions

region, the two-way nesting improves the CG as compared to the SA-C profile. An one-way nested simulation will not benefit from the higher surface resolution of the FG as there is no feedback to the CG.

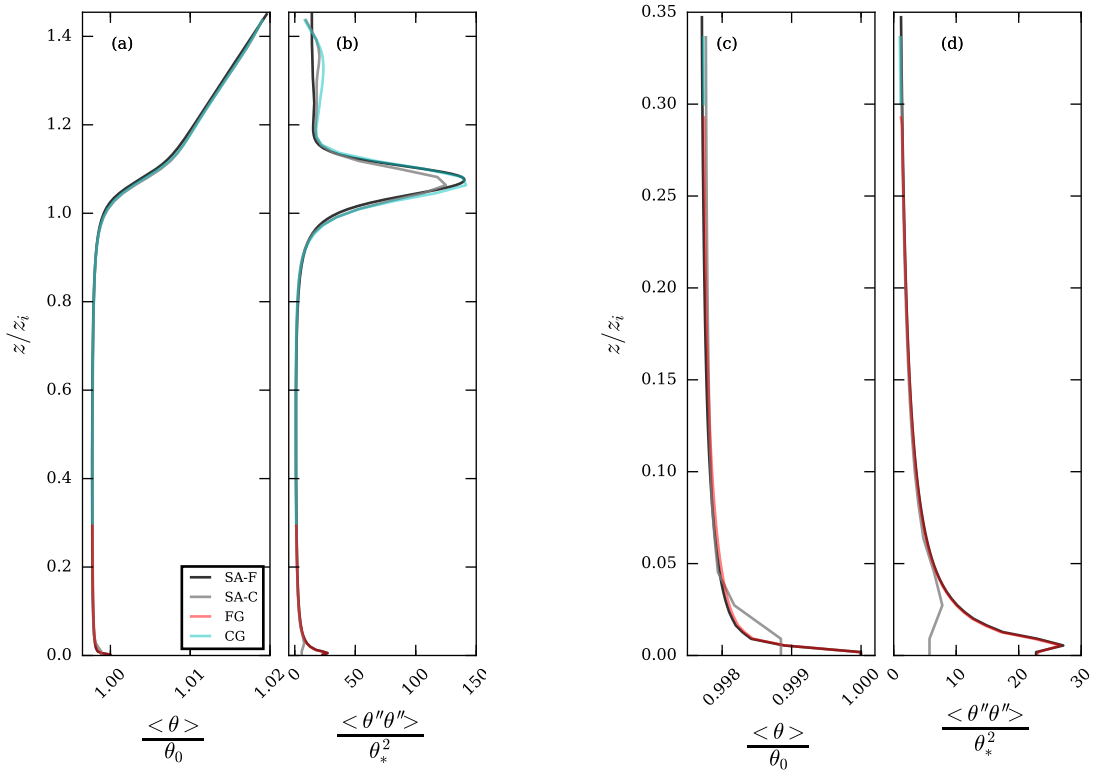

Figure 5. Vertical profile of horizontally averaged potential temperature normalized by surface value (a and c) and variance of potential temperature normalized by θ_*^2 (b and d). The nested grid profiles agree well with the SA-F in the surface layer. The improvement of the two-way nesting, at the boundary layer height, is seen in the good agreement in the profiles of CG and SA-F in (b).

The variance of u, v and w velocity components are plotted in Fig. 6. The u and v variance are normalized by the square of the friction velocity (u_*^2) and the w variance is normalized by the square of the convective velocity (w_*^2). The u and w FG profiles have a better agreement with the SA-F than the v variance. A marginal overshoot of the v variance seen in Fig. 6 (e). We can notice the remainder of a small kink in the vertical velocity variance at the nesting height. This is a side effect of the anterpolation and the magnitude of the kink can be minimized by using a sponge layer, see Sullivan et al. (1996). In our two-way nesting we have used a simplified sponge layer by limiting the anterpolation to one CG cell less than the nested height, this segregation of the anterpolation region in the CG and top boundary condition level of the FG provides reasonable reduction of kinks in the profile.

Geosci. Model Dev. Discuss., https://doi.org/10.5194/gmd-2018-287
Manuscript under review for journal Geosci. Model Dev.
Discussion started: 3 December 2018

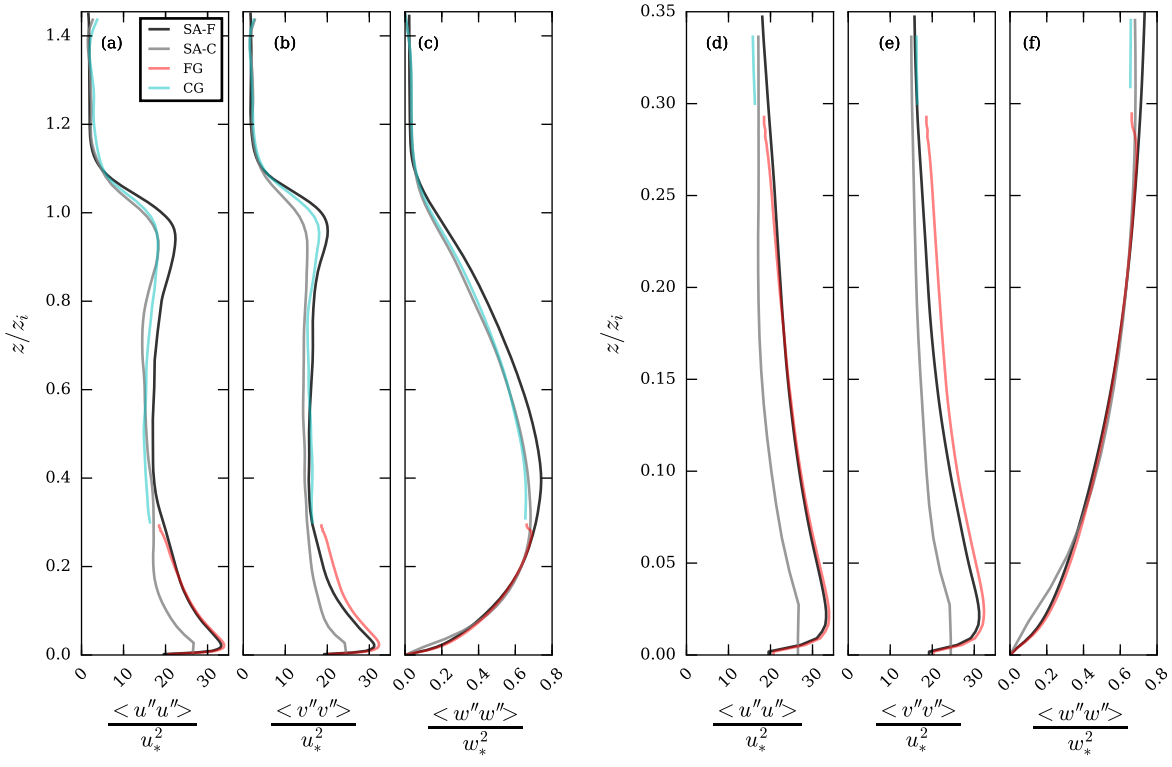

Figure 6. Vertical profile of horizontally averaged variance of u (a and d), v (b and e), and w (c and f). The horizontal velocity components are normalized by u_*^2 and the vertical velocity variance is normalized by w_*^2. The variance of u and w show better agreement with the standalone reference in the surface layer

The vertical heat flux profile is the prime quantity of interest in analysing surface layer simulations. In the $< w''\theta'' >$ profiles in Fig. 7, the FG have perfect agreement with the SA-F in the surface layer for the resolved, SGS and the total flux profiles. In the CG regions above the nested grid height, too a good agreement with the SA-C is found. The improvement due to the two-way nesting is seen in Fig. 7 (d and e), where the effects of low grid resolution of the SA-C in resolved and SGS fluxes are evident. However, no grid dependent difference in the profile is observed in the total flux.

Geosci. Model Dev. Discuss., https://doi.org/10.5194/gmd-2018-287
Manuscript under review for journal Geosci. Model Dev.
Discussion started: 3 December 2018

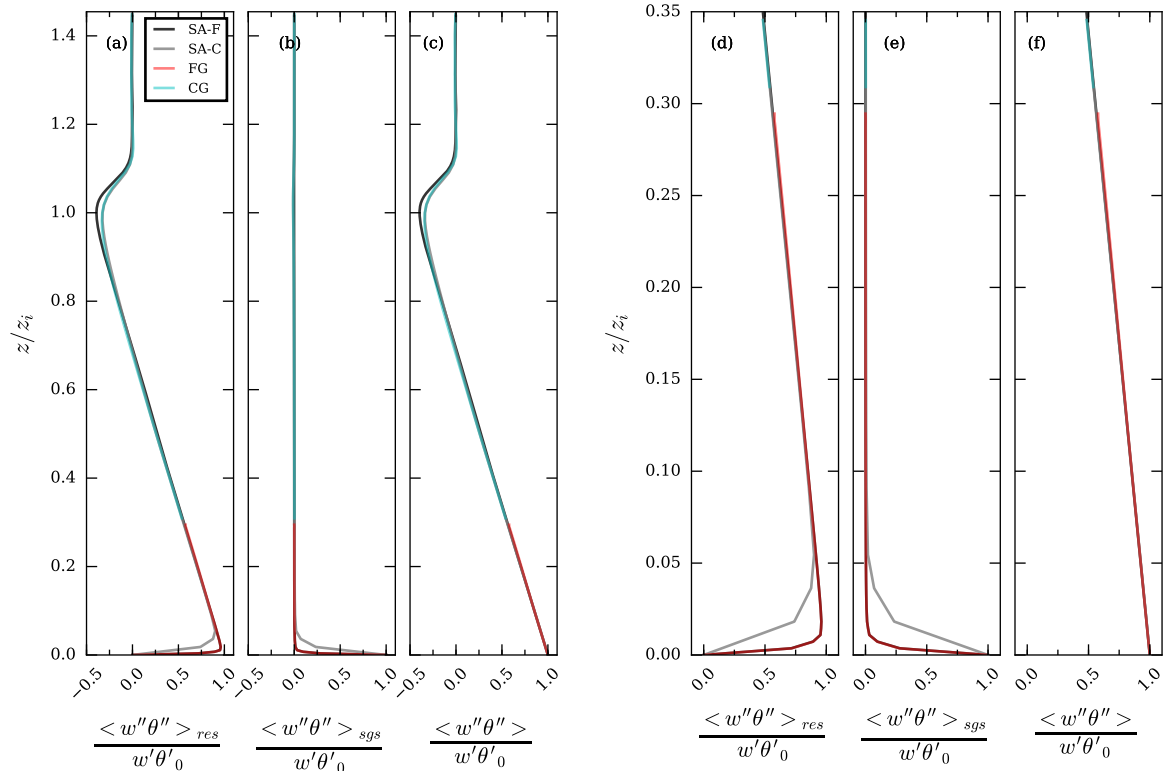

Figure 7. Vertical profile of horizontally averaged heat flux normalized by the surface heat flux – resolved (a and d), sub-grid (b and e), and total flux (c and f). The two-way nesting significantly improves the resolved and SGS fluxes in the surface layer.

3.3 Computational Performance

The computational resources used in the simulations discussed above are listed in Table 2. The resources needed by SA-C is only 5 core hours. While the nested simulations needed about 1450 core hours, the SA-F needed 7 times more core hours. If we increase the resolution further, the time step Δt will get smaller and consequently increase the total number of steps to be integrated. Simulations with O(1) m resolution become prohibitively expensive to achieve. The two-way nesting algorithm reduces the memory requirement and the number of core hours needed by providing higher resolution only in the surface layer.

Several factors influence the computational performance of an LES code. Some factors depend on the hardware, for e.g. number of grid points per PE depends on the memory available per node. On the other hand, the communication time for data exchange between the PEs depend on the topology of the domain decomposition. The best performance in terms of communication time in a standalone run is achieved when the number of sub-domains in the x and y directions are equal. In a nested simulation, the load per PE, i.e. the number of grid points per PE, in the two grids vary. As the speed of the model integration depends on the PE load, the load balancing between fine and coarse grid has an effect on the computational performance of the nested simulation. Keeping these factors in mind, we designed a new nested simulation domain to measure

Geosci. Model Dev. Discuss., https://doi.org/10.5194/gmd-2018-287
Manuscript under review for journal Geosci. Model Dev.
Discussion started: 3 December 2018

the computational performance as the total number of processors is varied. The number of grid points in the CG is around 2 x 10^8 and in the FG it is around 6.3 x 10^9. The ratio between the number of PEs for CG and FG is kept constant to avoid load balancing bias in the scaling. Keeping the processor ratio constant implies that the ratio between the number of grid points per PE in CG and FG are also held constant. Consequently, in this performance test, the FG has 1.25 times more grid points per PE than the CG in all the processor configurations tested. To compare the performance of nested model against the non-nested version of PALM under equivalent work load, a grid with the same dimensions of the FG is set-up. This non-nested grid also has the same load per PE and same number of cores as the FG. Such a non-nested set-up is acceptable for comparison since the number of PE in CG is negligible compared to the PE in FG in our set-up (e.g. 14400 PE in FG and only 576 PE in CG). A pure standalone simulation with FG resolution throughout the boundary layer was not performed as it would need about 25 x 10^9 grid points and such a large domain was computationally not feasible.

The performance is measured in terms of the time taken to simulate one time step. To increase the accuracy of this performance measurement, the simulation is integrated for ten time steps and the average of the time per step is plotted. The results presented in Fig. 8 shows close to linear scaling for up to 14976 PE in both nested and standalone runs. The difference in time per step between the nested and standalone runs can be interpreted as the additional computational time needed by the nesting algorithm. A jump in the time taken to compute one step is observed when more than 8192 PEs are used. This is a hardware dependent increase in communication time as the nodes are grouped as 'islands' on SuperMUC. The communication within the nodes of the same island is faster than the communication across multiple islands.

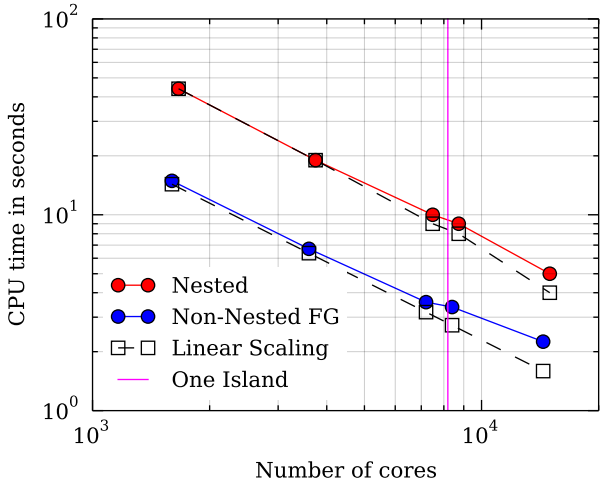

Figure 8. The nested simulations show close to linear scalability. A Non-Nested domain with same number of grid points as the FG is plotted to benchmark the scalability of the standard version of PALM on the same machine. The difference between the blue and the red line is approximately equal to the additional computational time needed by the nesting routines. The simulations were performed on SuperMUC at the Leibniz Supercomputing Center. Each node has 32 GB of main memory and two Sandy-Bridge processors with 2.7 GHz, each processor has 8 cores (Anastopoulos et al., 2013).

Geosci. Model Dev. Discuss., https://doi.org/10.5194/gmd-2018-287
Manuscript under review for journal Geosci. Model Dev.
Discussion started: 3 December 2018

Geoscientific Model Development Discussions
Open Access
EGU

3.4 Practical Considerations

In this paragraph we summarize some guidelines for using this nesting approach. In PALM, the user has the choice to select between Wicker-Skamarock (Wicker and Skamarock, 2002) and Piacsek-Williams (Piacsek and Williams, 1970) for advection scheme. Similarly, for solving Poisson equation for the pressure, the user can choose between the FFT or Multi-Grid based solver. During the development and the validation of the two-way nesting, only the Wicker-Skamarock advection scheme and FFT based pressure solvers were tested. The two-way nesting supports only periodic boundary conditions in the horizontal for both CG and FG, and therefore FFT based pressure solver is an appropriate choice. However, to be able to use Multi-Grid solvers, for e.g. in non-periodic horizontal boundary conditions, modifications to the two-way nesting algorithm will be needed. The large scale forcing feature in PALM is found to be compatible with the nesting algorithm without further modifications. Other features like canopy parameterization, radiation model, land surface models etc. have not been tested.

Our implementation of the vertical nesting allows only integer nesting ration in all directions. We recommend odd nesting ratio, in the range of 3 and 9, as the accuracy of the simulations decrease with the increase in nesting ratio. The height of the nested domain has a direct influence on the accuracy of the two-way nesting algorithm. Based on our trials (not shown) we recommend that the overlapping FG covers at least 12 grid levels of the CG. In an LES, the first five grid points are unreliable and this condition extends also to the FG. For better computational performance it is recommended that the number of grid points per PE in the CG is kept at only 40 to 80 percent of the FG value. The reduced work load of the CG minimizes the waiting time of the FG during the concurrent time advancement by quicker CG pressure solver step.

Though our nesting technique computationally makes feasible surface layer resolution down to 0.5 m for a moderately large domain care should be taken to ensure validity of such LES. In PALM, the height of the first grid point should be at the least twice greater than the local surface-roughness parameter. This technical restriction is common to all models that employ MOST and ensures proper evaluation of the logarithm needed in the calculation of u^*. Furthermore, Basu and Lacser (2017) recently recommended that MOST boundary-conditions should be adapted for very high-resolution LES where the first grid point is smaller than 2-5 times the height of the roughness elements.

4 Summary

We presented a two-way grid nesting technique that enables high resolution LES of the surface layer. In our concurrently parallel algorithm, the two grids with different resolution overlap in the region close to the surface. The grids are coupled at every sub-step of the Runge-Kutta time integration. The interpolation of the boundary conditions and the feedback to the parent grid are performed by energy conserving methods. The exchange of data between the two grids is achieved by MPI communication routines and the function calls are optimized for performance. Results of the convective boundary layer simulation show that grid nesting improves the vertical profiles of variance and the fluxes in the surface layer. In particular, the profiles of the vertical temperature flux are improved. Due to the two-way nesting, there is also an improvement in the coarse grid in the profile of potential temperature variance. The current vertical nesting only works with periodic boundary conditions and the same horizontal extent in both the domains. The nested simulation needs 7 times less computational time than a full high

resolution simulation for comparable accuracy in the surface layer. The scalability of the algorithm on up to 14976 CPUs is demonstrated.

5 Code availability

The PALM code is distributed under the GNU General Public License. The code (revision 2712) is available at https://palm.muk.uni-hannover.de/trac/browser/palm?rev=2712.

Author contributions. SH was the main developer of the model code, with FDR as side developer, SR supporting the code development and MM, SR and FDR supervising the development. The experiment was designed by SH, FDR, SR and MM and carried out by SH, who also performed the validation. Visualization was done by SH, and the original draft written by SH and FDR, with review and editing by SR and MM. Funding acquisition and administration by MM.

Acknowledgements. This work was conducted within the Helmholtz Young Investigators Group "Capturing all relevant scales of biosphere-atmosphere exchange – the enigmatic energy balance closure problem", which is funded by the Helmholtz-Association through the President's Initiative and Networking Fund, and by KIT. Computer resources for this project have been provided by the Leibniz Supercomputing Centre under grant: pr48la. We thank Gerald Steinfeld for sharing his original notes and code of a preliminary nesting method in PALM. We also thank Matthias Sühring and Farah Kanani-Sühring of the PALM group for their help in standardizing and porting the code, and we thank Michael Manhart for fruitful discussions.

References

Anastopoulos, N., Nikunen, P., and Weinberg, V.: Best Practice Guide - SuperMUC v1.0. PRACE - Partnership for Advanced Computing in Europe 2013, http://www.prace-ri.eu/best-practice-guide-supermuc-html, 2013.

Basu, S. and Lacser, A.: A Cautionary Note on the Use of Monin–Obukhov Similarity Theory in Very High-Resolution Large-Eddy Simulations, Boundary-Layer Meteorology, 163, 351–355, doi:10.1007/s10546-016-0225-y, 2017.

Boersma, B. J., Kooper, M. N., Nieuwstadt, F. T. M., and Wesseling, P.: Local grid refinement in large-eddy simulations, Journal of Engineering Mathematics, 32, 161–175, doi:10.1023/A:1004283921077, 1997.

Clark, T. L. and Farley, R. D.: Severe downslope windstorm calculations in two and three spatial dimensions using anelastic interactive grid nesting: A possible mechanism for gustiness, J Atmos Sci, 41, 329–350, doi:10.1175/1520-0469(1984)041<0329:SDWCIT>2.0.CO;2, 1984.

Clark, T. L. and Hall, W. D.: Multi-domain simulations of the time dependent Navier Stokes equation: Benchmark error analyses of nesting procedures, J Comput Phys, 92, 456–481, doi:10.1016/0021-9991(91)90218-A, 1991.

Daniels, M. H., Lundquist, K. A., Mirocha, J. D., Wiersema, D. J., and Chow, F. K.: A New Vertical Grid Nesting Capability in the Weather Research and Forecasting (WRF) Model, Monthly Weather Review, 144, 3725–3747, doi:10.1175/mwr-d-16-0049.1, 2016.

Deardorff, J. W.: Three-dimensional numerical study of the height and the mean structure of a heated planetary boundary layer, Bound-Layer Meteorol, 7, 81–106, doi:10.1007/BF00224974, 1974.

Deardorff, J. W.: Stratocumulus-capped mixed layers derived from a three-dimensional model, Bound.-Lay. Meteorol., 18, 495–527, doi:10.1007/BF00119502, 1980.

Debreu, L., Marchesiello, P., Penven, P., and Cambon, L.: Two-way nesting in split-explicit ocean models: Algorithms, implementation and validation, Ocean Modelling, 49-50, 1–21, doi:10.1016/j.ocemod.2012.03.003, 2012.

Esau, I.: Indirect air–sea interactions simulated with a coupled turbulence-resolving model, Ocean Dynamics, 64, 689–705, doi:10.1007/s10236-014-0712-y, 2014.

Germano, M., Piomelli, U., Moin, P., and Cabot, W. H.: A dynamic subgrid scale eddy viscosity model, Phys. Fluid A, 3, 7, doi:10.1063/1.857955, 1991.

Harris, L. M. and Durran, D. R.: An Idealized Comparison of One-Way and Two-Way Grid Nesting, Monthly Weather Review, 138, 2174–2187, doi:10.1175/2010mwr3080.1, 2010.

Kato, C., Kaiho, M., and Manabe, A.: An Overset Finite-Element Large-Eddy Simulation Method With Applications to Turbomachinery and Aeroacoustics, Journal of Applied Mechanics, 70, 32, doi:10.1115/1.1530637, 2003.

Khanna, S. and Brasseur, J. G.: Three-Dimensional Buoyancy- and Shear-Induced Local Structure of the Atmospheric Boundary Layer, Journal of the Atmospheric Sciences, 55, 710–743, doi:10.1175/1520-0469(1998)055<0710:tdbasi>2.0.co;2, 1998.

Kravchenko, A., Moin, P., and Moser, R.: Zonal Embedded Grids for Numerical Simulations of Wall-Bounded Turbulent Flows, Journal of Computational Physics, 127, 412–423, doi:10.1006/jcph.1996.0184, 1996.

Kröniger, K., De Roo, F., Brugger, P., Huq, Sadiq amd Banerjee, T., Zinsser, J., Rotenberg, E., Yakir, D., Rohatyn, S., and Mauder, M.: Effect of Secondary Circulations on the Surface-Atmosphere Exchange of Energy at an Isolated Semi-arid Forest, doi:10.1007/s10546-018-0370-6, 2018.

Manhart, M.: A zonal grid algorithm for DNS of turbulent boundary layers, Computers and Fluids, 33, 435–461, doi:10.1016/S0045-7930(03)00061-6, 2004.

Maronga, B., Gryschka, M., Heinze, R., Hoffmann, F., Kanani-Sühring, F., Keck, M., Ketelsen, K., Letzel, M. O., Sühring, M., and Raasch, S.: The Parallelized Large-Eddy Simulation Model (PALM) version 4.0 for atmospheric and oceanic flows: model formulation, recent developments, and future perspectives, Geoscientific Model Development, 8, 2515–2551, doi:10.5194/gmd-8-2515-2015, 2015.

Moeng, C.-H. and Wyngaard, J. C.: Spectral analysis of large-eddy simulations of the convective boundary layer, J. Atmos. Sci., 45, 3573–3587, doi:10.1175/1520-0469(1988)045<3573:SAOLES>2.0.CO;2, 1988.

Moeng, C.-H., Dudhia, J., Klemp, J., and Sullivan, P.: Examining Two-Way Grid Nesting for Large Eddy Simulation of the PBL Using the WRF Model, Mon Wea Rev, 135, 2295–2311, doi:10.1175/MWR3406.1, 2007.

Nakahashi, K., Togashi, F., and Sharov, D.: Intergrid-Boundary Definition Method for Overset Unstructured Grid Approach, AIAA Journal, 38, 2077–2084, doi:10.2514/2.869, 2000.

Patton, E. G., Sullivan, P. P., Shaw, R. H., Finnigan, J. J., and Weil, J. C.: Atmospheric Stability Influences on Coupled Boundary Layer and Canopy Turbulence, Journal of the Atmospheric Sciences, 73, 1621–1647, doi:10.1175/jas-d-15-0068.1, 2016.

Piacsek, S. A. and Williams, G. P.: Conservation properties of convection difference schemes, J. Comput. Phys., 198, 500–616, doi:10.1016/0021-9991(70)90038-0, 1970.

Raasch, S. and Schröter, M.: PALM - A large-eddy simulation model performing on massively parallel computers, Meteorologische Zeitschrift, 10, 363–372, doi:10.1127/0941-2948/2001/0010-0363, 2001.

Reynolds, W. C.: The potential and limitations of direct and large eddy simulations, in: Whither Turbulence? Turbulence at the Crossroads, edited by Lumley, J. L., pp. 313–343, Springer Berlin Heidelberg, Berlin, Heidelberg, doi:10.1007/3-540-52535-1_52, 1990.

Saiki, E. M., Moeng, C.-H., and Sullivan, P. P.: Large-eddy simulation of the stably stratified planetary boundary layer, Bound.-Lay. Meteorol., 95, 1–30, doi:10.1023/A:1002428223156, 2000.

Schmidt, H. and Schumann, U.: Coherent structure of the convective boundary layer derived from large-eddy simulations, J Fluid Mech, 200, 511–562, doi:10.1017/S0022112089000753, 1989.

Skamarock, W., Klemp, J., Dudhia, J., Gill, D., Barker, D., Wang, W., Huang, X.-Y., and Duda, M.: A Description of the Advanced Research WRF Version 3, doi:10.5065/d68s4mvh, 2008.

Sullivan, P. P., McWilliams, J. C., and Moeng, C.-H.: A grid nesting method for large-eddy simulation of planetary boundary layer flows, Bound-Layer Meteorol, 80, 167–202, doi:10.1007/BF00119016, 1996.

Wang, G., Duchaine, F., Papadogiannis, D., Duran, I., Moreau, S., and Gicquel, L. Y.: An overset grid method for large eddy simulation of turbomachinery stages, Journal of Computational Physics, 274, 333–355, doi:10.1016/j.jcp.2014.06.006, 2014.

Wicker, L. J. and Skamarock, W. C.: Time-splitting methods for elastic models using forward time schemes, Mon. Wea. Rev., 130, 2008–2097, doi:10.1175/1520-0493(2002)130<2088:TSMFEM>2.0.CO;2, 2002.

Williamson, J. H.: Low-storage Runge-Kutta schemes, J. Comput. Phys., 35, 48–56, doi:10.1016/0021-9991(80)90033-9, 1980.

Zhou, B., Xue, M., and Zhu, K.: A Grid-Refinement-Based Approach for Modeling the Convective Boundary Layer in the Gray Zone: Algorithm Implementation and Testing, Journal of the Atmospheric Sciences, 75, 1143–1161, doi:10.1175/jas-d-17-0346.1, 2018.